Available online at www.sciencedirect.com
ScienceDirect
Atmospheric Environment 41 (2007) 934–949
ATMOSPHERIC ENVIRONMENT
www.elsevier.com/locate/atmosenv

# Modeling reactive pollutant dispersion in an urban street canyon

Jong-Jin Baik[a,*], Yoon-So Kang[a], Jae-Jin Kim[b,1]

[a]*School of Earth and Environmental Sciences, Seoul National University, Seoul 151-742, Republic of Korea*
[b]*Numerical Weather Prediction Division, Korea Meteorological Administration, Seoul 156-720, Republic of Korea*

Received 10 May 2006; received in revised form 11 September 2006; accepted 15 September 2006

**Abstract**

Reactive pollutant dispersion in an urban street canyon with a street aspect ratio of one is numerically investigated using a computational fluid dynamics (CFD) model. The CFD model developed is a Reynolds-averaged Navier–Stokes equations (RANS) model with the renormalization group (RNG) $k$–$\varepsilon$ turbulence model and includes transport equations for NO, $NO_2$, and $O_3$ with simple photochemistry. An area emission source of NO and $NO_2$ is considered in the presence of background $O_3$ and street bottom heating ($\Delta T = 5\,^{\circ}C$) with an ambient wind perpendicular to the along-canyon direction. A primary vortex is formed in the street canyon and the line connecting the centers of cross-sectional vortices meanders over time and in the canyon space. The cross-canyon-averaged temperature and reactive pollutant concentrations oscillate with a period of about 15 min. The averaged temperature is found to be in phase with NO and $NO_2$ concentrations but out of phase with $O_3$ concentration. The photostationary state defect is small in the street canyon except for near the roof level and the upper downwind region of the canyon and its local minimum is observed near the center of the primary vortex. The budget analysis of NO ($NO_2$) concentration shows that the magnitude of the advection or turbulent diffusion term is much larger (larger) than that of the chemical reaction term and that the advection term is largely balanced by the turbulent diffusion term. On the other hand, the budget analysis of $O_3$ concentration shows that the magnitude of the chemical reaction term is comparable to that of the advection or turbulent diffusion term. The inhomogeneous temperature distribution itself affects $O_3$ concentration to some extent due to the temperature-dependent photolysis rate and reaction rate constant.


*Keywords:* Computational fluid dynamics (CFD) model; Urban street canyon; Street bottom heating; Reactive pollutant dispersion; Photochemistry

## 1. Introduction

Flow and dispersion in urban street canyons have been widely investigated during the past two decades because of their practical implications as well as fluid dynamical interest. This research has been undertaken through field observations (e.g., DePaul and Sheih, 1986; Rotach, 1995; Eliasson et al., 2006), fluid experiments using wind tunnels or water tanks (e.g., Brown et al., 2000; Caton et al., 2003; Liu et al., 2003), and computational fluid dynamics (CFD) model simulations (e.g., Hunter et al., 1992; Kim and Baik, 2004; Tsai et al., 2005). The CFD modeling approach as a way to understand

*Corresponding author. Tel.: +82 2 880 6990; fax: +82 2 883 4972.
*E-mail address:* jjbaik@snu.ac.kr (J.-J. Baik).
[1]Present address: Department of Environmental Atmospheric Sciences, Pukyong National University, Busan 608-737, Republic of Korea.

1352-2310/$ - see front matter © 2006 Elsevier Ltd. All rights reserved.
doi:10.1016/j.atmosenv.2006.09.018

street canyon flow and dispersion has become powerful and comprehensive with recent advances in computing power, numerical method/algorithm, and turbulence parameterization. Previous CFD modeling studies have contributed to our understanding of the many important aspects of street canyon flow and dispersion. These include flow regime (Hunter et al., 1992; Jeong and Andrews, 2002), mean flow and turbulence statistics (Rotach, 1995; Liu and Barth, 2002), dispersion mechanism (Baik and Kim, 2002), thermal effects on flow and dispersion (Sini et al., 1996; Xie et al., 2005; Tsai et al., 2005), and bulk effects of buildings on mean flow and turbulent kinetic energy (Zhang et al., 2006).

In previous CFD modeling studies of dispersion in urban street canyons, passive (non-reactive) pollutant (scalar) was exclusively considered and its concentration was calculated using a prognostic equation for the passive pollutant. In urban areas, a main pollutant source is automobiles and the pollutants emitted from automobiles, for example NO and $NO_2$, are chemically reactive. Complex photochemical processes in densely built-up urban areas with heavy traffic often result in a serious air pollution problem. Therefore, to further enhance our understanding of street canyon dispersion, reactive pollutants need to be taken into account. Recently, Baker et al. (2004) introduced the simple photochemistry of NO–$NO_2$–$O_3$ into a large-eddy simulation model and examined reactive pollutant dispersion in a street canyon with a street aspect ratio of one. It was shown that the photostationary state defect is a sensitive indicator of reactive mixing in the street canyon and its value is small near the center of the primary vortex. In their study, a thermodynamic energy equation was not included and accordingly the photolysis rate and reaction rate constant should be specified as values at a given temperature.

When the street bottom or building surfaces are heated by solar radiation, in-canyon temperature distribution becomes non-uniform. The temperature and its distribution pattern are dependent upon the degree of street bottom or building surface heating, the geometry of buildings and street canyons, and meteorological conditions (Kim and Baik, 2001). Hence, in the case of street bottom or building surface heating it is natural to treat reaction coefficients as temperature-dependent. In this CFD modeling study, we extend the work of Baker et al. (2004) by taking temperature-dependent reaction coefficients into account and investigate reactive pollutant dispersion in an urban street canyon with bottom heating. For this study, we have developed a CFD model with a thermodynamic energy equation and prognostic equations for the reactive pollutants NO, $NO_2$, and $O_3$, performed numerical simulations with and without street bottom heating, and analyzed simulation data.

## 2. Numerical model

The CFD model developed for this study is based upon the Reynolds-averaged Navier–Stokes equations (RANS) model (Kim and Baik, 2004) that includes the renormalization group (RNG) $k-\varepsilon$ turbulence model proposed by Yakhot et al. (1992). The RNG $k-\varepsilon$ turbulence model was shown to improve upon the standard $k-\varepsilon$ turbulence model in simulating turbulent kinetic energy field near the upwind edge of the building (Kim and Baik, 2004). To investigate reactive pollutant dispersion in the presence of street bottom heating, a thermodynamic energy equation and transport equations for reactive pollutants are implemented into the RANS model. The momentum equation, mass continuity equation, and thermodynamic energy equation under the Boussinesq approximation are given by

$$\frac{\partial U_i}{\partial t}+U_j\frac{\partial U_i}{\partial x_j}=-\frac{1}{\rho_0}\frac{\partial P^*}{\partial x_i}+\delta_{i3}g\frac{T^*}{T_0}+\nu\frac{\partial^2 U_i}{\partial x_j\partial x_j}-\frac{\partial}{\partial x_j}(\overline{u_iu_j}), \tag{1}$$

$$\frac{\partial U_j}{\partial x_j}=0, \tag{2}$$

$$\frac{\partial T}{\partial t}+U_j\frac{\partial T}{\partial x_j}=\kappa\frac{\partial^2 T}{\partial x_j\partial x_j}-\frac{\partial}{\partial x_j}(\overline{T'u_j})+S_{\mathrm{h}}. \tag{3}$$

Here, $U_i$ is the $i$th mean velocity component, $T$ the mean temperature, $u_i$ the fluctuation from $U_i$, $T'$ the fluctuation from $T$, $P^*$ the deviation of pressure from its reference value, $T^*$ the deviation of temperature from its reference value ($=T-T_0$), $\rho_0$ the air density, $\delta_{ij}$ the Kronecker delta, $g$ the gravitational acceleration, $\nu$ the kinematic viscosity of air, and $\kappa$ the thermal diffusivity of air. $S_{\mathrm{h}}$ in (3) denotes the source/sink term of heat.

The Reynolds stress and turbulent heat flux in (1) and (3) are parameterized using

$$-\overline{u_i u_j} = K_m\left(\frac{\partial U_i}{\partial x_j}+\frac{\partial U_j}{\partial x_i}\right)-\frac{2}{3}\delta_{ij}k, \tag{4}$$

$$-\overline{T' u_j} = K_h\frac{\partial T}{\partial x_j}, \tag{5}$$

where $K_m$ is the eddy (or turbulent) viscosity of momentum, $K_h$ the eddy diffusivity of heat, and $k$ the turbulent kinetic energy. In the RNG $k-\varepsilon$ turbulence model, $K_m$ is expressed by

$$K_m = \nu\left(1+\left(\frac{C_\mu}{\nu}\right)^{1/2}\frac{k}{\varepsilon^{1/2}}\right)^2, \tag{6}$$

where $C_\mu$ is an empirical constant and $\varepsilon$ the dissipation rate of turbulent kinetic energy. The Prandtl number Pr ($=K_m/K_h$) is specified as 0.7. $K_m$ is computed using the prognostic equations of turbulent kinetic energy and its dissipation rate.

$$\frac{\partial k}{\partial t}+U_j\frac{\partial k}{\partial x_j} = -\overline{u_i u_j}\frac{\partial U_i}{\partial x_j}+\frac{\delta_{3j}g}{T_0}\overline{T' u_j} + \frac{\partial}{\partial x_j}\left(\frac{K_m}{\sigma_k}\frac{\partial k}{\partial x_j}\right)-\varepsilon, \tag{7}$$

$$\frac{\partial \varepsilon}{\partial t}+U_j\frac{\partial \varepsilon}{\partial x_j} = -C_{\varepsilon 1}\frac{\varepsilon}{k}\overline{u_i u_j}\frac{\partial U_i}{\partial x_j}+C_{\varepsilon 1}\frac{\varepsilon}{k}\frac{\delta_{3j}g}{T_0}\overline{T' u_j} + \frac{\partial}{\partial x_j}\left(\frac{K_m}{\sigma_\varepsilon}\frac{\partial \varepsilon}{\partial x_j}\right)-C_{\varepsilon 2}\frac{\varepsilon^2}{k}-R, \tag{8}$$

where $\sigma_k$, $\sigma_\varepsilon$, $C_{\varepsilon 1}$, and $C_{\varepsilon 2}$ are empirical constants. The last term in (8) is an extra strain rate term given by

$$R = \frac{C_\mu \eta^3(1-\eta/\eta_0)\varepsilon^2}{(1+\beta_0\eta^3)k}, \tag{9}$$

$$\eta = \frac{k}{\varepsilon}\left[\left(\frac{\partial U_i}{\partial x_j}+\frac{\partial U_j}{\partial x_i}\right)\frac{\partial U_i}{\partial x_j}\right]^{1/2}. \tag{10}$$

Following Yakhot et al. (1992), the constants in the RNG $k-\varepsilon$ turbulence model are specified as

$$(C_\mu,\ \sigma_k,\ \sigma_\varepsilon,\ C_{\varepsilon 1},\ C_{\varepsilon 2},\ \beta_0,\ \eta_0) = (0.0845,\ 0.7179,\ 0.7179,\ 1.42,\ 1.68,\ 0.012,\ 4.377). \tag{11}$$

The reactive pollutants we are concerned with in this study are nitric oxide (NO) and nitrogen dioxide ($NO_2$), which are supposed to be emitted from automobiles into the street canyon in the presence of background ozone ($O_3$) and sunlight. The chemical reactions considered are

$$NO_2 + h\nu \rightarrow NO + O, \tag{12}$$

$$O + O_2 + M \rightarrow O_3 + M, \tag{13}$$

$$O_3 + NO \rightarrow NO_2 + O_2. \tag{14}$$

In (13), M represents a molecule ($N_2$ or $O_2$ or another third molecule) that absorbs excess energy and thereby stabilizes $O_3$ molecule formed (Seinfeld and Pandis, 1998). The sunlight with wavelength $\lambda<420$ nm photodissociates $NO_2$ to NO and $NO_2$ is reproduced through the reaction of $O_3$ with NO (Carpenter et al., 1998). Then, transport equations for NO, $NO_2$, and $O_3$ can be expressed by

$$\frac{\partial [NO]}{\partial t}+U_j\frac{\partial [NO]}{\partial x_j} = D\frac{\partial^2 [NO]}{\partial x_j \partial x_j}+\frac{\partial}{\partial x_j}\left(K_c\frac{\partial [NO]}{\partial x_j}\right) + J_{NO_2}[NO_2]-k_1[O_3][NO]+S_{NO}, \tag{15}$$

$$\frac{\partial [NO_2]}{\partial t}+U_j\frac{\partial [NO_2]}{\partial x_j} = D\frac{\partial^2 [NO_2]}{\partial x_j \partial x_j}+\frac{\partial}{\partial x_j}\left(K_c\frac{\partial [NO_2]}{\partial x_j}\right) - J_{NO_2}[NO_2]+k_1[O_3][NO]+S_{NO_2}, \tag{16}$$

$$\frac{\partial [O_3]}{\partial t}+U_j\frac{\partial [O_3]}{\partial x_j} = D\frac{\partial^2 [O_3]}{\partial x_j \partial x_j}+\frac{\partial}{\partial x_j}\left(K_c\frac{\partial [O_3]}{\partial x_j}\right) + k_2[O][O_2][M]-k_1[O_3][NO], \tag{17}$$

where $D$ is the molecular diffusivity of the pollutants, $K_c$ the eddy diffusivity of the pollutants, $J_{NO_2}$ the photolysis rate of $NO_2$ in (12), $k_1$ the rate constant for the reaction in (14), and $k_2$ the rate constant for the reaction in (13). $S_{NO}$ and $S_{NO_2}$ denote the source terms of NO and $NO_2$, respectively. The Schmidt number Sc ($=K_m/K_c$) is specified as 0.9. Seinfeld and Pandis (1998) state that the oxygen atom is highly reactive, so that its depletion rate by (13) is equal to its formation rate by (12). This is the so-called pseudo-steady-state approximation for a highly reactive chemical species. Thus,

$$k_2[O][O_2][M] = J_{NO_2}[NO_2]. \tag{18}$$

Then, (17) may be rewritten as

$$\frac{\partial[O_3]}{\partial t} + U_j\frac{\partial[O_3]}{\partial x_j} = D\frac{\partial^2[O_3]}{\partial x_j \partial x_j} + \frac{\partial}{\partial x_j}\left(K_c\frac{\partial[O_3]}{\partial x_j}\right) + J_{NO_2}[NO_2] - k_1[O_3][NO]. \quad (19)$$

Adding (15) and (16) [(16) and (19)] reveals that $NO + NO_2$ ($= NO_x$) [$NO_2 + O_3$ ($= OX$)] is effectively passive (Baker et al., 2004) because the chemical reaction terms cancel each other out. The photolysis rate $J_{NO_2}$ and reaction rate constant $k_1$ are temperature-dependent and calculated using (Shetter et al., 1988; Seinfeld and Pandis, 1998; Baker et al., 2004)

$$J_{NO_2} = 8.14\times10^{-3}\{0.97694 + 8.3700\times10^{-4} \times(T-273.15) + 4.5173\times10^{-6}(T-273.15)^2\}, \quad (20)$$

$$k_1 = 44.05\times10^{-3}\exp\left(-\frac{1370}{T}\right), \quad (21)$$

where $T$ is in K and the units of $J_{NO_2}$ and $k_1$ are $s^{-1}$ and $ppb^{-1}\ s^{-1}$, respectively.

The above governing equations. (1)–(3), (7), (8), (15), (16), and (19) are numerically solved using a finite volume method with the semi-implicit method for pressure-linked equation (SIMPLE) algorithm (Patankar, 1980). Details of the numerical procedure are described in Baik et al. (2003). Notice that the numerical procedure to solve prognostic equations for the reactive pollutants is the same as that to solve a prognostic equation for the passive pollutant that is described in detail in Baik et al. (2003). It is known that major difficulties in chemistry modeling are generally nonlinear chemistry and very fast chemical reactions. In the present simple photochemistry modeling, however, there is no difficulty in solving (15), (16), and (19) numerically with the pseudo-steady-state approximation (18).

## 3. Experimental setup and model initialization

Fig. 1 illustrates the computational domain and building configuration. This study models reactive pollutant dispersion in an infinitely long street canyon when the ambient wind direction ($x$-direction) is perpendicular to the along-canyon direction ($y$-direction). The origin of the coordinate system is located at the center of the street bottom in the computational domain. The domain size is 40 m in the $x$-direction, 50 m in the $y$-direction ($L$), and

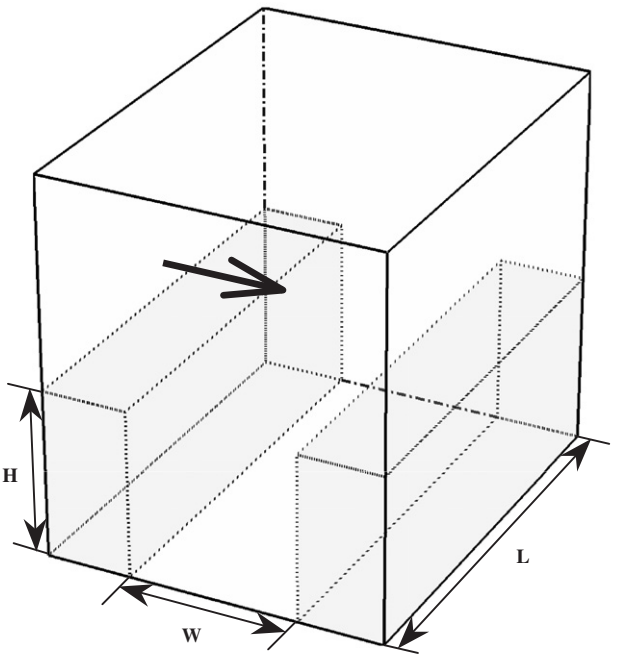


Fig. 1. An illustration of the computational domain and building configuration. $H$ is the building height, $W$ the width between two buildings, $L$ the domain size in the along-canyon direction. The ambient wind direction is perpendicular to the along-canyon direction.

60.1 m in the $z$-direction. The building height $H$ is 20 m and the width between two buildings $W$ is 20 m, giving a street aspect ratio of one. The grid intervals are uniform in the horizontal with $\Delta x = 0.5$ m and $\Delta y = 1$ m. In the vertical, the grid interval is uniform up to $z = 32$ with $\Delta z = 0.5$ m and then increases with an expansion ratio of 1.1. The model is integrated for 2 h with a time step of 0.1 s.

At the inflow boundary, ambient wind speed, directed in the $x$-axis, and turbulent kinetic energy and its dissipation rate are specified as (Castro and Apsley, 1997)

$$U_{\text{in}}(z) = \frac{u_*}{\kappa} \ln\left(\frac{z}{z_0}\right), \tag{22}$$

$$k_{\text{in}}(z) = \frac{1}{C_\mu^{1/2}} u_*^2 \left(1 - \frac{z}{\delta}\right)^2, \tag{23}$$

$$\varepsilon_{\text{in}}(z) = \frac{C_\mu^{3/4} k_{\text{in}}^{3/2}}{\kappa z}, \tag{24}$$

where $u_*$, $z_0$, $\delta$, and $\kappa$ are the friction velocity, roughness length, boundary-layer depth, and von Karman constant, respectively. The initial and inflow-boundary air temperature is set at 25 °C and the temperature of the street bottom is fixed at 30 °C during the model integration. This imitates street bottom heating by solar radiation. At the outflow, spanwise, and upper boundaries, zero-gradient boundary conditions are applied. The wall boundary conditions for momentum and heat are applied at the solid surface (Versteeg and Malalasekera, 1995).

There is considered to be an area emission source in this study and pollutants are emitted at each grid cell of the lowest model level ($z = 0.25$ m). Here, an area emission source rather than line emission sources is considered simply because we want to investigate flow and reactive pollutant dispersion in a simpler framework. The initialization method for the reactive pollutants follows that of Baker et al. (2004). For the first 30 min of model integration ($t = 0$–30 min), no NO and $NO_2$ emissions exist. For the next 30 min ($t = 30$–60 min), passive pollutants are emitted at a rate of 50 ppb s$^{-1}$ per grid cell. At $t = 60$ min, NO concentration at each grid cell of the computational domain is set to be the passive pollutant concentration at that time and $NO_2$ concentration to be one-tenth of the NO concentration, following typical automobile emission ratios of NO to $NO_2$. For ozone concentration at $t = 60$ min, if NO concentration is not equal to zero, $O_3$ concentration is calculated using the photostationary state relation of $[O_3] = J_{NO_2}[NO_2]/k_1[NO]$ (Carpenter et al., 1998). If NO concentration is equal to zero (in practice a very small value), $O_3$ concentration is specified as 20 ppb. For $t = 60$–120 min, NO and $NO_2$ are emitted at rates of 50 and 5 ppb s$^{-1}$, respectively, per grid cell. A NO emission rate of 50 ppb s$^{-1}$ per grid cell corresponds to 613 μg s$^{-1}$ m$^{-1}$ and a $NO_2$ emission rate of 5 ppb s$^{-1}$ per grid cell corresponds to 94 μg s$^{-1}$ m$^{-1}$. Considering a $NO_x$ emission of 0.5 g km$^{-1}$ per vehicle (Baker et al., 2004), a $NO_x$ emission of 707 μg s$^{-1}$ m$^{-1}$ is equivalent to about 5100 vehicles per hour. This is a case of heavy traffic. The problem of validating the numerical model is given in the last part of the next section.

## 4. Results and discussion

Two numerical experiments with and without street bottom heating are performed and simulation data are analyzed. Fig. 2 shows the $x$–$z$ cross section of streamline and temperature fields at $y = -0.5$ m ($y/H = -0.025$, $x$–$z$ plane closest to the center of the model street canyon) and $t = 92.5$ min in the case of street bottom heating. A primary vortex in clockwise rotation is formed in the street canyon and a small, counterclockwise rotating vortex is produced near the bottom corner of the downwind building. At this time, the temperature near the upwind building wall is higher than that near the downwind building wall because of the temperature advection towards the upwind building wall by the reversed flow in the lower region of the canyon.

Fig. 3 shows the vertical profiles of vertical velocity at an upwind location of $x/H = -0.3125$ and $y/H = -0.025$ and a downwind location of $x/H = 0.3125$ and $y/H = -0.025$ at $t = 92.5$ min. Both the upward motion at the upwind location and the downward motion at the downwind location (except for the region above $z/H = 0.875$ in Fig. 3b) are stronger in the case of bottom heating than in the case of no heating. This is because thermally induced upward motion near the upwind building wall due to the positive buoyancy is constructively combined with mechanically induced upward motion formed when there is no heating, thus resulting in stronger upward motion there and consequently a strengthened vortex circulation in the street canyon.

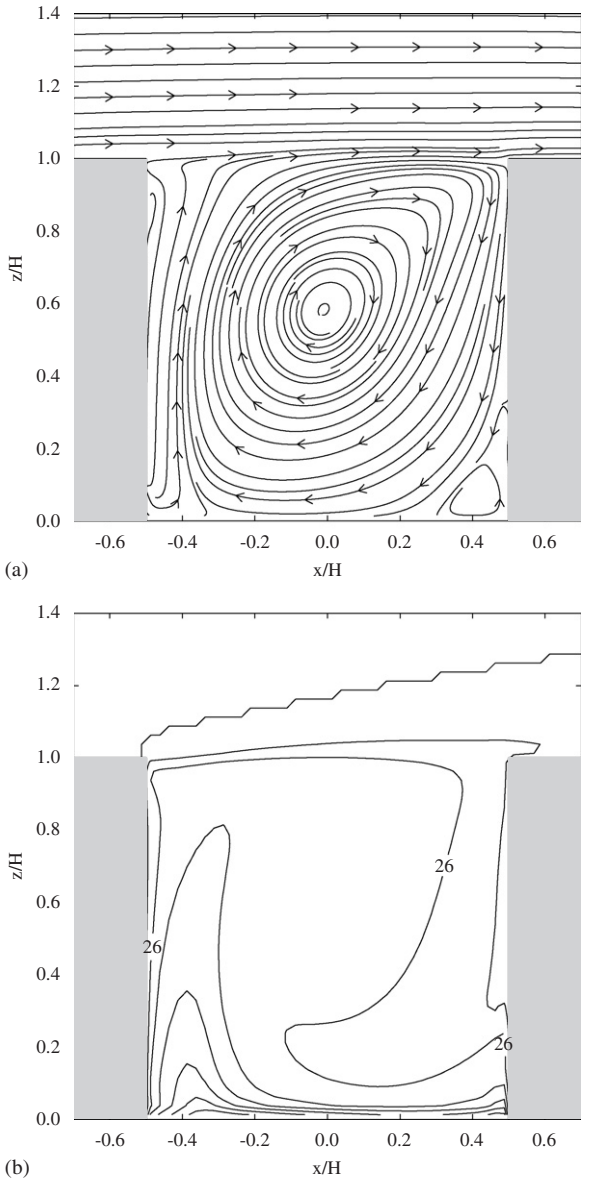


Fig. 2. (a) Streamline and (b) temperature fields at $y = -0.5$ m ($y/H = -0.025$) and $t = 92.5$ min in the case of street bottom heating. The contour interval in (b) is 0.5 °C.

This is consistent with many previous studies of thermal effects on urban street canyon flows (e.g., Kim and Baik, 1999; Bohnenstengel et al., 2004; Xie et al., 2005). It is, however, noticed that at any instant the magnitude of vertical velocity near the upwind/downwind building wall is not always larger in the case of bottom heating than in the case of no heating because the vortex center in the case of bottom heating meanders over time and in the canyon space, as shown below.

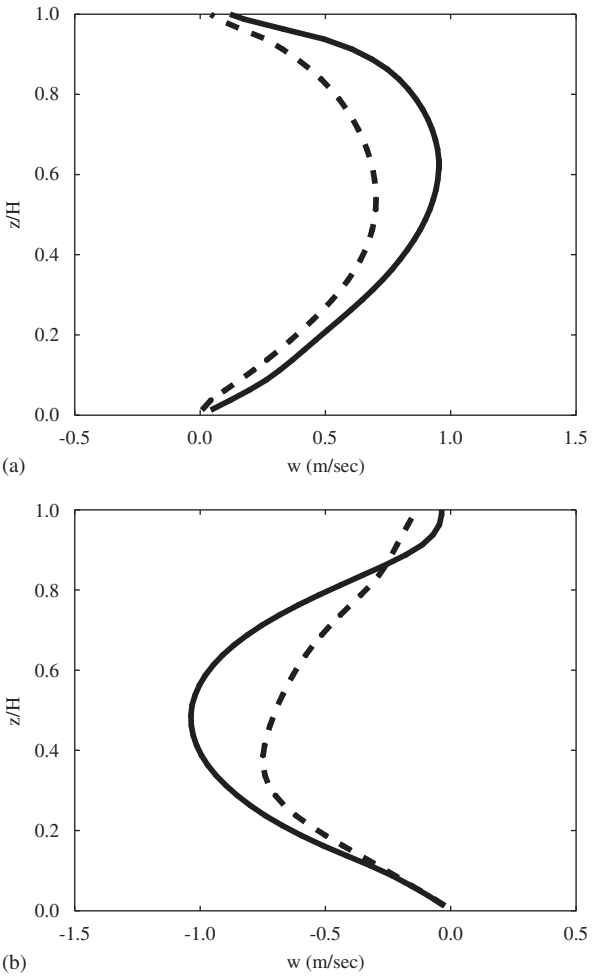


Fig. 3. Vertical profiles of vertical velocity at (a) ($x/H$, $y/H$) = (−0.3125, −0.025) and (b) ($x/H$, $y/H$) = (0.3125, −0.025) in the cases of no heating (dashed line) and street bottom heating (solid line). These profiles are at $t = 92.5$ min.

Fig. 4 shows vortex lines connecting the centers of $x-z$ cross-sectional vortices in the street canyon at $t = 90.5$ and 95 min. When there is no heating, the vortex line is straight and there is no spatial variation (dashed line in Fig. 4). Furthermore, the location of the vortex line does not change with time (see Figs. 5a and b). On the other hand, when there is street bottom heating, the vortex line exhibits a spatial variation in the street canyon (solid line in Fig. 4) and the vortex center of each $x-z$ cross section meanders over time (see Figs. 5a and b). The spatial and temporal variation of the vortex line is essentially related to three-dimensional thermal instability caused by bottom heating. A similar behavior of the vortex line in three dimensions is

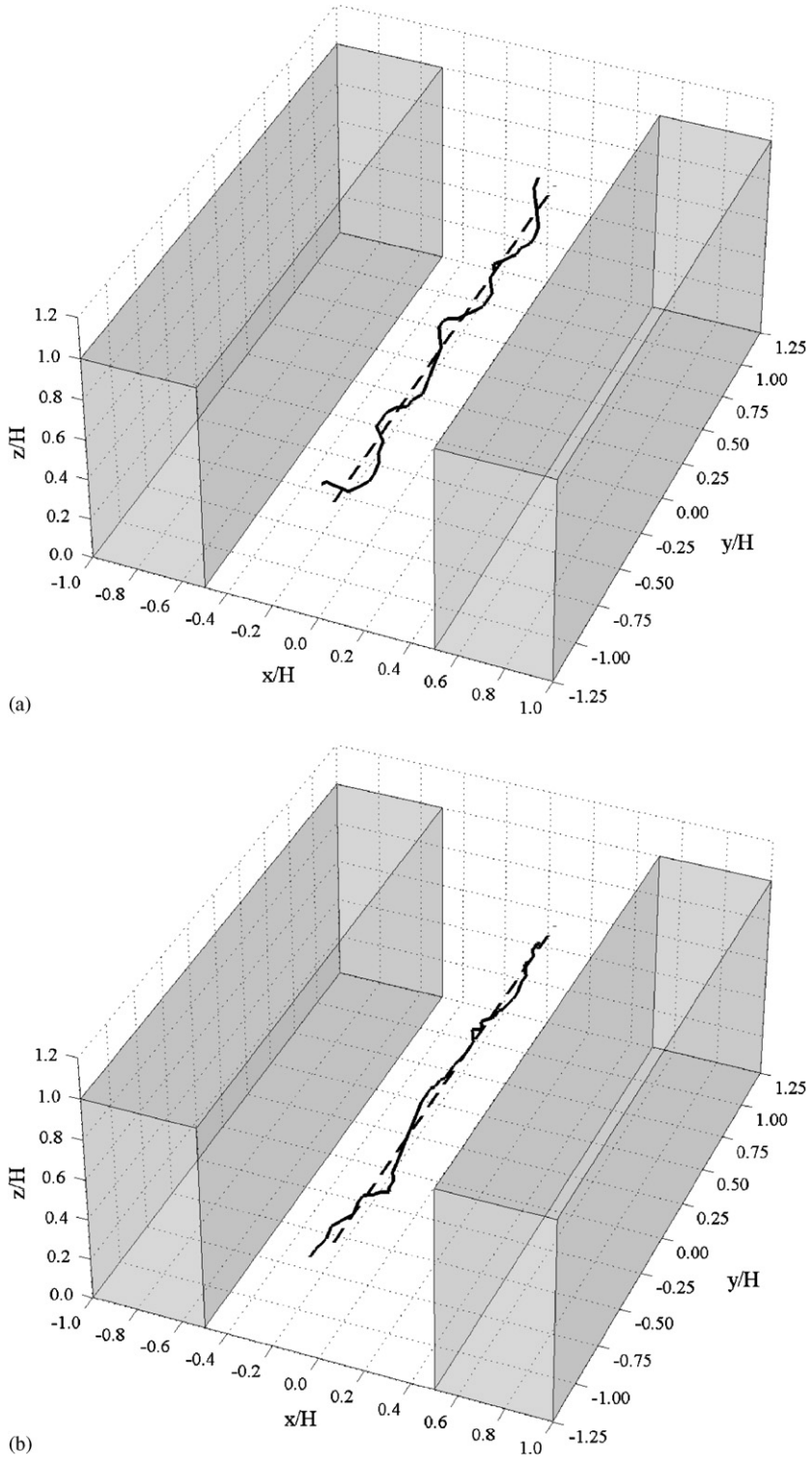


Fig. 4. Vortex lines connecting the centers of $x-z$ cross-sectional vortices in the street canyon at (a) $t = 90.5$ min and (b) $t = 95$ min in the cases of no heating (dashed line) and street bottom heating (solid line).

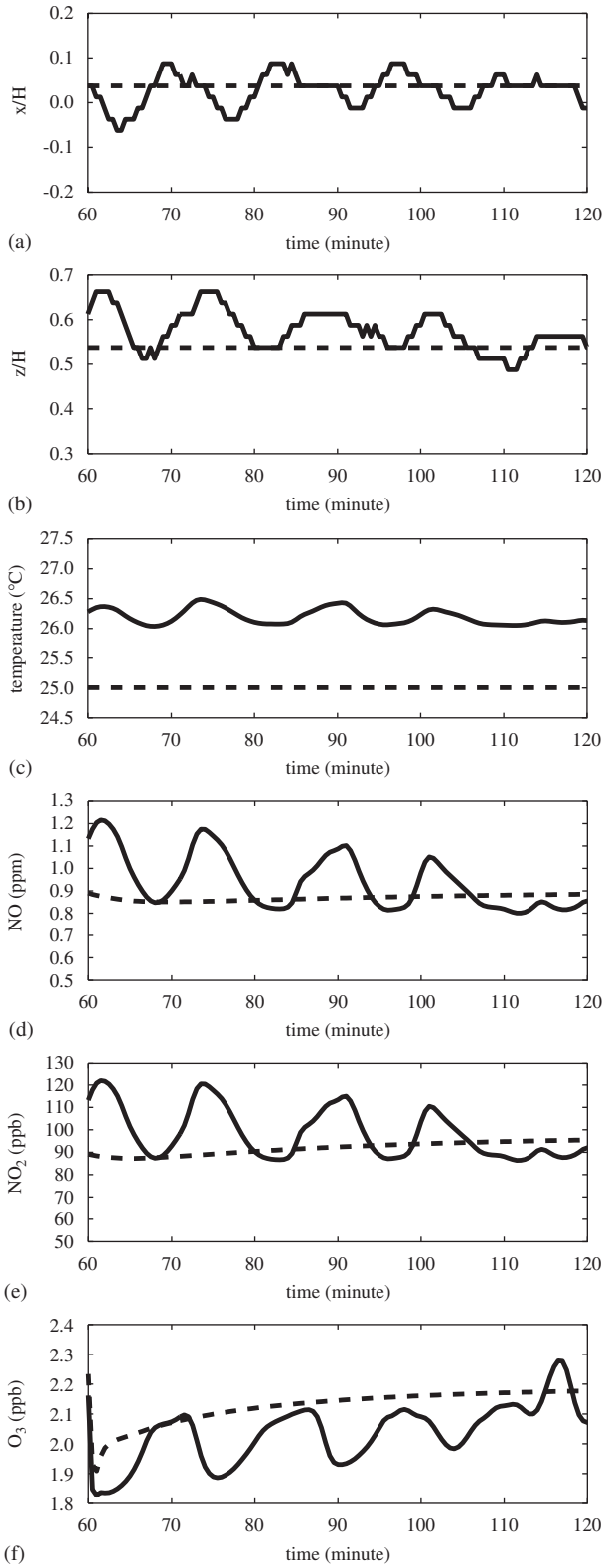


Fig. 5. Time series of (a) $x$-location, and (b) $z$-location of vortex center and street canyon-averaged, (c) temperature, (d) NO concentration, (e) $NO_2$ concentration, and (f) $O_3$ concentration at $y/H = -0.025$ in the cases of no heating (dashed line) and street bottom heating (solid line).

simulated in a street canyon formed by two buildings (Tsai et al., 2005).

Fig. 5 shows the time series of the horizontal and vertical locations of vortex center and street canyon-averaged temperature and reactive pollutant concentrations at $y/H = -0.025$. Here, the average is taken over a domain (plane) of $-0.5 \leqslant x/H \leqslant 0.5$ and $0 \leqslant z/H \leqslant 1$ at $y/H = -0.025$. Notice that NO concentration is in ppm and $NO_2$ and $O_3$ concentrations are in ppb. When there is no heating, the location of vortex center does not change with time and the temperature is 25 °C everywhere. The reactive pollutant concentrations after $t = \sim 70$ min increase slightly with time and then remain nearly constant near the end of time integration. When there is bottom heating, the vortex center meanders in the street canyon and the canyon-averaged temperature and reactive pollutant concentrations oscillate with time. A spectral analysis of the time series data showed a dominant peak at about 15 min (an oscillation period of about 15 min).

The canyon-averaged NO and $NO_2$ concentrations at $y/H = -0.025$ tend to be higher in the case of bottom heating than in the case of no heating (Figs. 5d and e). This result seems to contradict previous two-dimensional studies indicating that the pollutant concentration in the street canyon tends to become lower in the presence of bottom heating (e.g., Kim and Baik, 1999; Xie et al., 2005). In the present three-dimensional simulation with a street bottom heating intensity of $\Delta T = 5$ °C, it is, however, found that the canyon-averaged NO and $NO_2$ concentrations can be either higher or lower in the case of bottom heating depending on the $x$–$z$ cross-sectional location (see Figs. 6b and c). This is associated with a spatial variation in the vortex center in the along-canyon direction. It is observed from Figs. 5c–e that in the case of bottom heating the averaged temperature is in phase with the averaged NO and $NO_2$ concentrations. When the temperature is high (low), the vortex center rises (lowers) in the vertical (Fig. 5b) and consequently the flow becomes weak (strong) in the canyon region below the vortex center. Thus, NO and $NO_2$, whose sources are located near the street bottom, can stay longer (shorter) in the street canyon. This results in high (low) NO and $NO_2$ concentrations. This explains the positive phase relation between the canyon-averaged temperature and NO and $NO_2$ concentrations. It is also observed from Figs. 5c–f that the averaged $O_3$ concentration is out of phase with the averaged temperature, NO concentration, and $NO_2$ concentration.

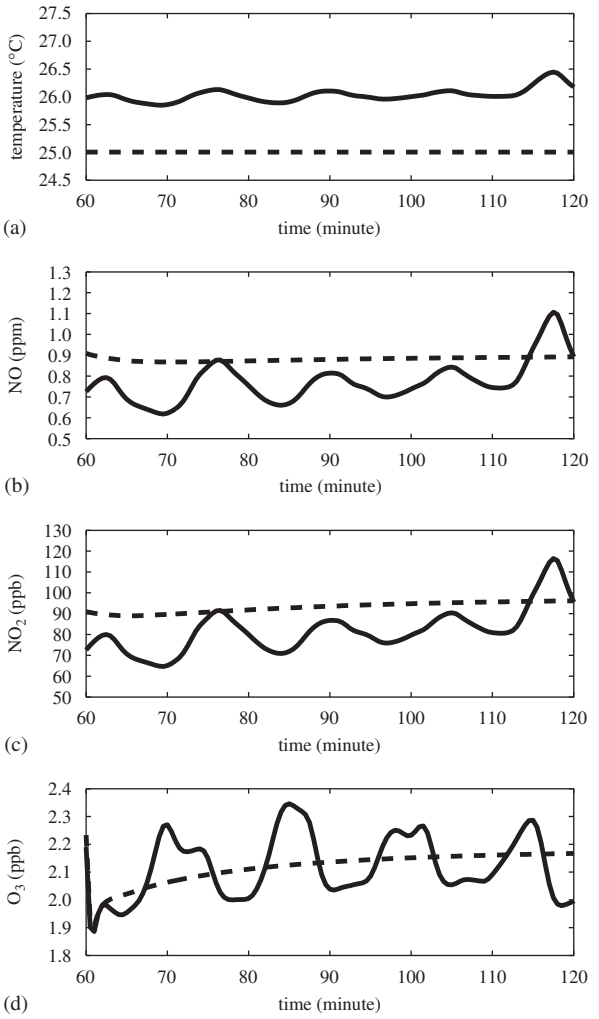


Fig. 6. Time series of street canyon-averaged (a) temperature, (b) NO concentration, (c) $NO_2$ concentration, and (d) $O_3$ concentration at $y/H = -0.625$ in the cases of no heating (dashed line) and street bottom heating (solid line).

The time series of street canyon-averaged temperature and reactive pollutant concentrations at $y = -12.5$ m ($y/H = -0.625$) are presented in Fig. 6. As is the case for $y/H = -0.025$, the canyon-averaged temperature and NO, $NO_2$, and $O_3$ concentrations oscillate with a period of about 15 min. Until $t = 114$ min, the canyon-averaged temperature is slightly lower at $y/H = -0.625$ than at $y/H = -0.025$ and its amplitude is also smaller at $y/H = -0.625$ than at $y/H = -0.025$ (Fig. 5c and 6a). At this $x$–$z$ cross-sectional plane, the canyon-averaged NO ($NO_2$) concentration in the case of street bottom heating is lower than that in the case

of no heating [Fig. 6b (Fig. 6c)] except for near the end of time integration. The canyon-averaged temperature is in phase with the canyon-averaged NO and $NO_2$ concentrations but approximately out of phase with the canyon-averaged $O_3$ concentration. This feature is also observed at $y/H = -0.025$ (Fig. 5).

It is interesting in Figs. 5 and 6 to observe the oscillatory behavior in the time series of the vortex center location and the averaged temperature and reactive pollutant concentrations. To examine whether the oscillatory behavior is due to a dynamical characteristic of flow in the presence of street bottom heating, four numerical experiments were performed. In each numerical experiment, only one factor differs from the experiment with street bottom heating in Figs. 2–6. In the first experiment, the grid interval is increased twice ($\Delta x = 1$ m, $\Delta y = 2$ m, and $\Delta z = 1$ m). In the second experiment, the time step is halved ($\Delta t = 0.05$ s). In the third experiment, the temperature-independent $J_{NO_2}$ and $k_1$ (their values at 25 °C are used) are considered. In the fourth experiment, a prognostic equation for the passive pollutant instead of prognostic equations for the reactive pollutants is numerically solved particularly to see whether the chemical reactions are responsible for the oscillation. The analysis of simulation data showed that the oscillation does appear in all the experiments, suggesting that a dynamical characteristic of flow in the presence of street bottom heating is responsible for the oscillation.

Figs. 5 and 6 show that the oscillation does not appear when there is no street bottom heating, but appears when the street bottom heating intensity is 5 °C. This result implies that the oscillation depends on street bottom heating intensity ($\Delta T$). Extensive numerical experiments have been conducted with a wide range of $\Delta T$. Preliminary results indicate that the oscillation starts when $\Delta T$ exceeds a certain value, but in some range of $\Delta T$ the oscillation disappears and that the oscillation period is not the same in a range of $\Delta T$ and some cases have more than one spectral peak. Detailed analysis results will be reported later.

The building configuration shown in Fig. 1 implicitly considers an infinitely long street canyon. A numerical experiment was performed in which the building length in the along-canyon direction is 25 m (a finite building length of 25 m). In this case, it was found that the street canyon-averaged temperature and reactive pollutant concentrations do not oscillate with time. This implies that the oscillatory behavior depends on building configuration. A further study with different building configurations, ambient wind directions, boundary conditions, and so on is needed to investigate under what situations/conditions the oscillation appears or does not appear.

The time series of street canyon-averaged $NO + NO_2$ ($= NO_x$) concentration at $y/H = -0.025$ and $-0.625$ in the case of street bottom heating were plotted and examined. The oscillation in the time series was also observed. This is because $NO + NO_2$ ($= NO_x$) is effectively passive and a dynamical

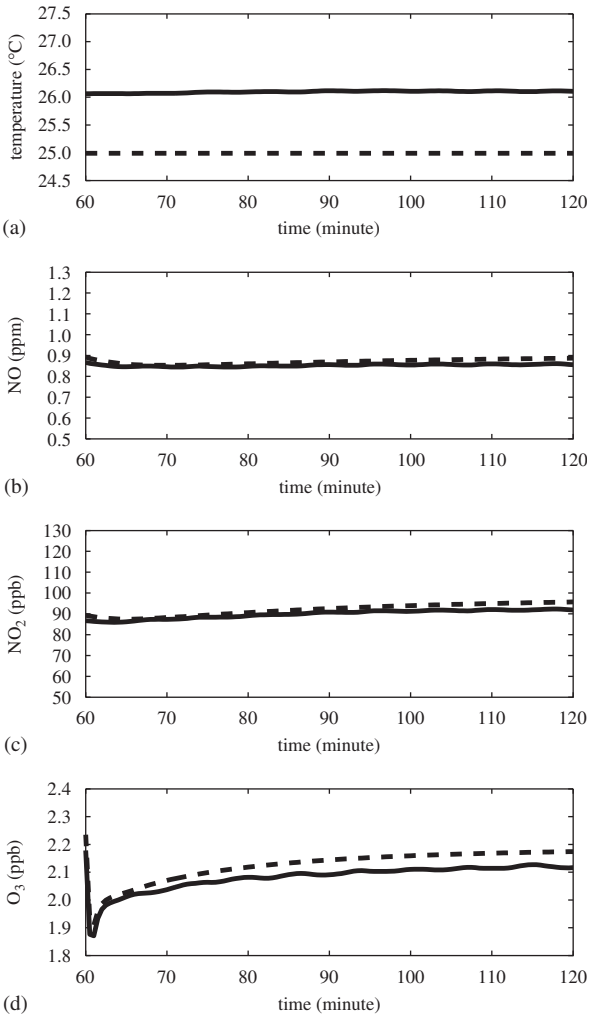


Fig. 7. Time series of (a) temperature, (b) NO concentration, (c) $NO_2$ concentration, and (d) $O_3$ concentration averaged over the entire street canyon in the cases of no heating (dashed line) and street bottom heating (solid line).

characteristic of flow in the presence of street bottom heating is responsible for the oscillation.

To examine the gross thermal effects on pollutant escape from the street canyon, the temporal variations of the entire street canyon-averaged temperature and reactive pollutant concentrations are plotted in Fig. 7. The average is taken over a model street canyon bounded by $-0.5 \leqslant x/H \leqslant 0.5$, $-1.25 \leqslant y/H \leqslant 1.25$, and $0 \leqslant z/H \leqslant 1$. The canyon-averaged temperature shows a very slight increase and then virtually no change (solid line in Fig. 7a), implying that the heat supplied from the street bottom is not accumulated over time in the street canyon but effectively transported and diffused into the above-canyon region. The canyon-averaged temperature is 26.1 °C, 1.1 °C higher than in the case of no heating. The canyon-averaged NO (also $NO_2$ and $O_3$) concentration is slightly lower in the case of street bottom heating than in the case of no heating.

The along-canyon- and time-averaged reactive pollutant concentration fields in the case of street bottom heating are shown in Figs. 8a–c. The average is taken along the street canyon ($-1.25 \leqslant y/H \leqslant 1.25$) and for $t = 83.0$–$97.5$ min. The time period corresponds to about one oscillation period in the time series of the reactive pollutant concentrations (Figs. 5 and 6). The spatial distribution pattern in the NO and $NO_2$ concentration fields reflects the existence of a primary vortex in the street canyon, that is, the concentration is higher near the upwind building than near the downwind building. Near the street bottom, NO and $NO_2$ concentrations are higher near the corner of the downwind building than near the street center since a small vortex formed near the corner (Fig. 2) recirculates

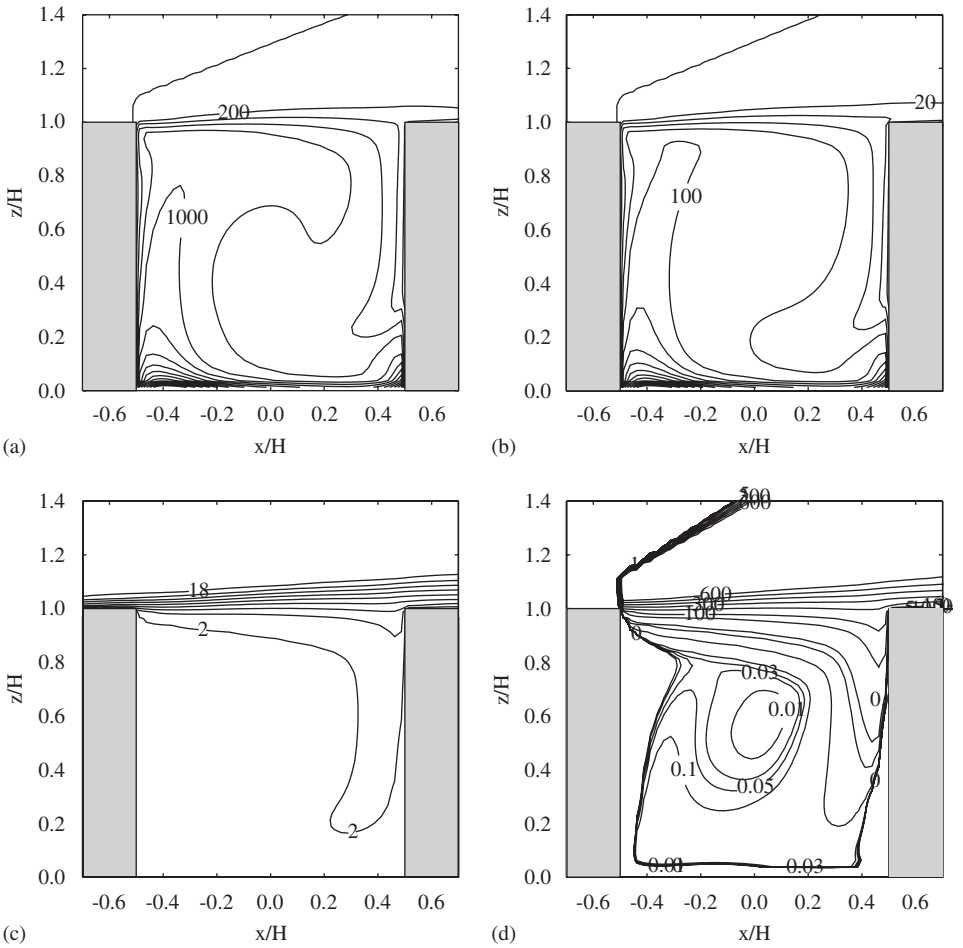


Fig. 8. Along-canyon- and time-averaged fields of (a) NO, (b) $NO_2$, and (c) $O_3$ concentrations (in ppb) and (d) photostationary state defect (%) in the case of street bottom heating. The average is taken over $-1.25 \leqslant y/H \leqslant 1.25$ and $83.0\,\text{min} \leqslant t \leqslant 97.5\,\text{min}$. The contour intervals in (a), (b), and (c) are 200, 20, and 2 ppb, respectively. The contour intervals in (d) are not uniform.

emitted pollutants therein. $O_3$ concentration is high near the upper downwind region of the street canyon where ambient ozone intrudes into the canyon.

Following Carpenter et al. (1998) and Baker et al. (2004), the photostationary state defect (%) is defined as

$$d_{ps} = \left(\frac{k_1[O_3][NO]}{J_{NO_2}[NO_2]} - 1\right) \times 100. \quad (25)$$

$d_{ps}$ contains the ratio of $O_3$ depletion rate to $O_3$ formation rate and is a measure of the departure degree from chemical equilibrium. When there is chemical equilibrium, $d_{ps}$ is zero. Fig. 8d shows along-canyon- and time-averaged photostationary state defect field in the case of street bottom heating. The photostationary state defect is small in the street canyon except for near the roof level and the upper downwind region of the canyon. There is a sharp rise in the photostationary state defect across the roof level of the street canyon. A local minimum in the photostationary state defect is observed near the center of the primary vortex because the circulatory flow speed there is weak and hence the recirculating pollutants have sufficient time to allow thorough mixing and reaction of the chemical species. In the street canyon, the photostationary state defect is large in the upper downwind region of the canyon. This is due to intruded background ozone being largely depleted through its chemical reaction with recirculating NO in the canyon. These simulated features in the photostationary state defect are similar to those of Baker et al. (2004). The photostationary state defect averaged over the entire street canyon and for a time period of 83.0–97.5 min is 7.4% in the case of no heating and 8.0% in the case of street bottom heating, increasing chemical disequilibrium when there is street bottom heating.

Next, a budget analysis of the reactive pollutants in the case of street bottom heating is performed to examine the role and relative importance of each process. Fig. 9 shows the along-canyon- and time-averaged ($-1.25 \leqslant y/H \leqslant 1.25$ and $83.0\,\text{min} \leqslant t \leqslant 97.5\,\text{min}$) fields of advection, turbulent diffusion, and chemical reaction terms in the transport equation for each reactive pollutant [(15), (16), and (19)]. To help interpret budget analysis results, the advection and turbulent diffusion terms are partitioned into components in the $x$, $y$, and $z$ directions (figures not shown).

In the budget analysis of NO equation, the magnitudes of the advection term, $-U_j\partial[NO]/\partial x_j$, and the turbulent diffusion term, $\partial/\partial x_j(K_c\partial[NO]/\partial x_j)$, are much larger than the magnitude of the chemical reaction term, $J_{NO_2}[NO_2] - k_1[O_3][NO]$. The magnitudes of the advection and turbulent diffusion terms are large in the outer region of the primary vortex. It is observed that the advection term is largely balanced by the turbulent diffusion term. Just below the roof level of the street canyon, positive NO advection acts to increase NO concentration and the turbulent diffusion process acts to reduce NO concentration. Partitioning each term into components indicates that just below the roof level NO depletion by the vertical turbulent diffusion process is to a large extent compensated for NO replenishment by the advection process through the primary vortex circulation. In the region close to the street bottom, negative NO advection acts to reduce NO concentration. In that region, the turbulent diffusion process acts to reduce NO concentration in the layer adjacent to the street bottom and increase NO concentration in the layer above it. Near the roof level, NO depletion rate is larger than its formation rate by photolysis of $NO_2$, so the chemical reaction process acts to reduce NO concentration there, but its contribution to the total NO concentration is minor. In the shallow layer above the downwind building top, the chemical reaction process is active because $O_3$ is abundant and NO and $NO_2$ concentrations are not very low (see Fig. 8).

The $NO_2$ budget calculation shows that the spatial distribution pattern of the advection term (turbulent diffusion term) is very similar to that in the NO budget, but its magnitude is much smaller. The chemical reaction term near the roof level acts to increase $NO_2$ concentration there. Notice that the chemical reaction term in the $NO_2$ transport equation has the same magnitude as, but the opposite sign to, that in the NO transport equation [see (15) and (16)]. In the $O_3$ budget, the magnitudes of the advection, turbulent diffusion, and chemical reaction terms are small in the street canyon but large across the roof level. The magnitude of the chemical reaction term is comparable to that of the advection (turbulent diffusion) term. Just below the roof level, the vertical turbulent diffusion process acts to increase $O_3$ concentration. The opposite behavior is observed in the NO and $NO_2$ budgets. This can be explained by the fact that NO and $NO_2$ escape from the street canyon (their emission source is located at the lowest model

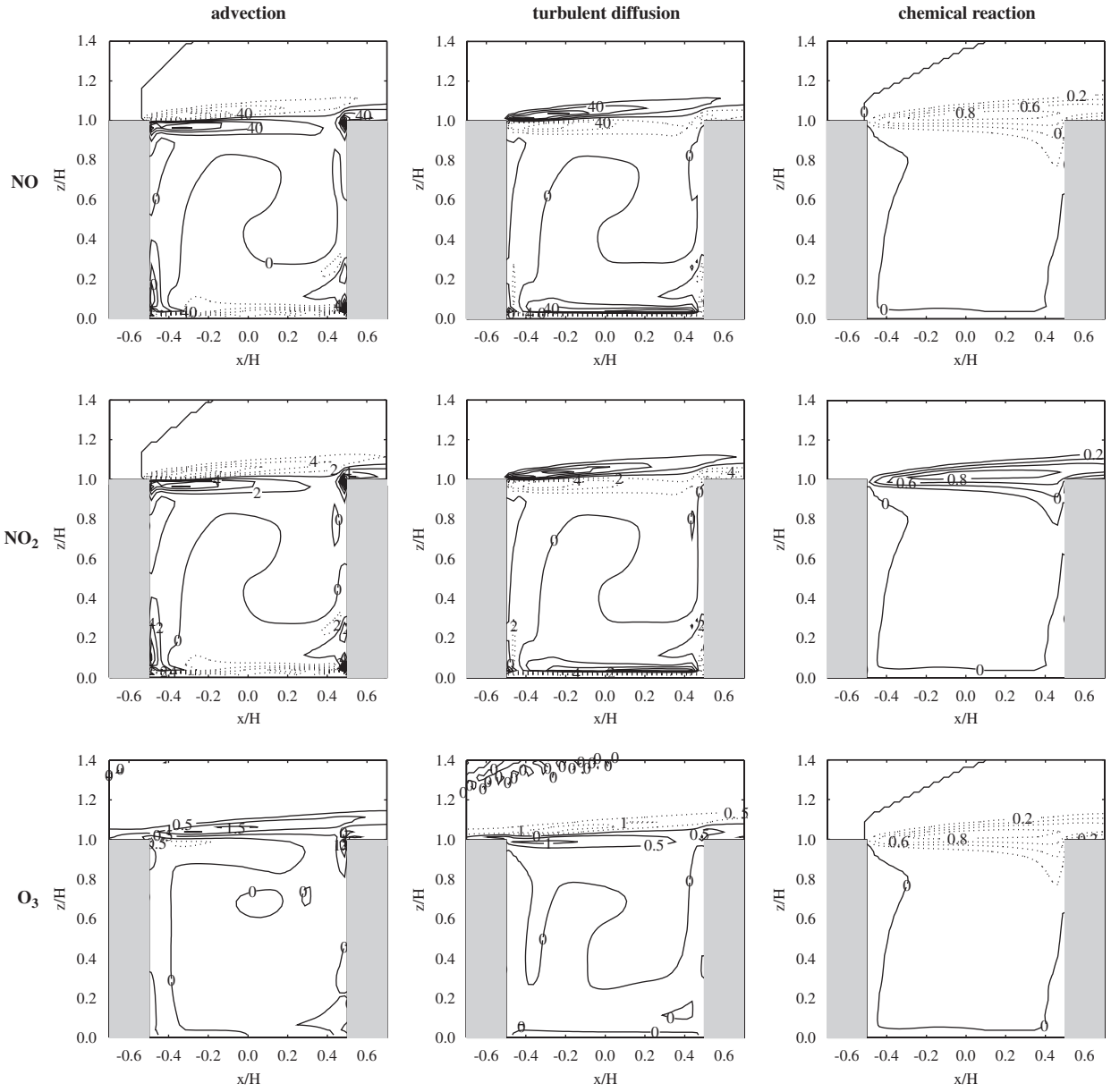


Fig. 9. Along-canyon- and time-averaged fields of advection, turbulent diffusion, and chemical reaction terms in the transport equations for the reactive pollutants in the case of street bottom heating. Figures in the upper, middle, and lower rows are for NO, $NO_2$, and $O_3$, respectively, and figures in the left, middle, and right columns are for advection, turbulent diffusion, and chemical reaction terms, respectively. The unit is ppb $s^{-1}$. The average is taken over $-1.25 \leqslant y/H \leqslant 1.25$ and $83.0\,\text{min} \leqslant t \leqslant 97.5\,\text{min}$. The contour interval in each figure is uniform.

level), while ambient $O_3$ enters into the street canyon. Near the roof level, the chemical reaction term acts to reduce $O_3$ concentration.

The photolysis rate $J_{NO_2}$ and the reaction rate constant $k_1$ are temperature-dependent. Hence, the inhomogeneous temperature distribution itself in the street canyon may affect the dispersion of the reactive pollutants there. To get some insight into this, simulation results from the experiment in the presence of street bottom heating, in which $J_{NO_2}$ and $k_1$ are temperature-independent (their values at 25 °C are used), are compared to those in the case with temperature-dependent $J_{NO_2}$ and $k_1$ (that is, the case of street bottom heating presented above).

To quantify results, a fractional difference in $O_3$ concentration between the two cases is computed. The fractional difference averaged over the entire street canyon and a given period (83.0 min $\leqslant t \leqslant$ 97.5 min) is 1.5%. This value is not negligibly small. In addition, the fractional difference field averaged along the street canyon and over the oscillation period shows that the fractional difference in the street canyon is relatively large near the street bottom and the lower upwind building where the temperature is high due to the street bottom heating and primary vortex circulation. The largest fractional difference is 5.0% at $x/H = -0.3375$ and $z/H = 0.0125$. Therefore, we conclude that with a street bottom heating intensity of $\Delta T = 5\,^{\circ}\mathrm{C}$ the inhomogeneous temperature distribution itself in the street canyon affects in-canyon ozone concentration to some extent by temperature-dependent $J_{NO_2}$ and $k_1$.

No experimental data on reactive pollutant concentration in a street canyon are available currently, so the present CFD model with simple photochemistry cannot be validated. However, experimental data on flow and temperature fields in a street canyon with street bottom heating are available. So, comparisons are made with available experimental data, as in Kim and Baik (2001). Fig. 9 shows the vertical profiles of normalized temperature and normalized streamwise horizontal velocity in a numerical simulation with a street bottom heating intensity of $\Delta T = 2\,^{\circ}\mathrm{C}$ and in the wind tunnel experiment of Uehara et al. (2000) with a bulk Richardson number of $-0.21$. The calculated bulk Richardson number in the numerical simulation is $-0.24$, similar to that in the wind tunnel experiment. The vertical profile of the normalized temperature in the numerical simulation follows that in the wind tunnel experiment. The vertical profiles of the normalized streamwise horizontal velocity are similar to each other except in the region below $z/H = 0.1$ and in the region near $z/H = 1.2$. The discrepancy in the region below $z/H = 0.1$ is to a large extent related to the wall boundary condition at the solid surface in the numerical simulation and the smooth model-street bottom in the wind tunnel experiment.

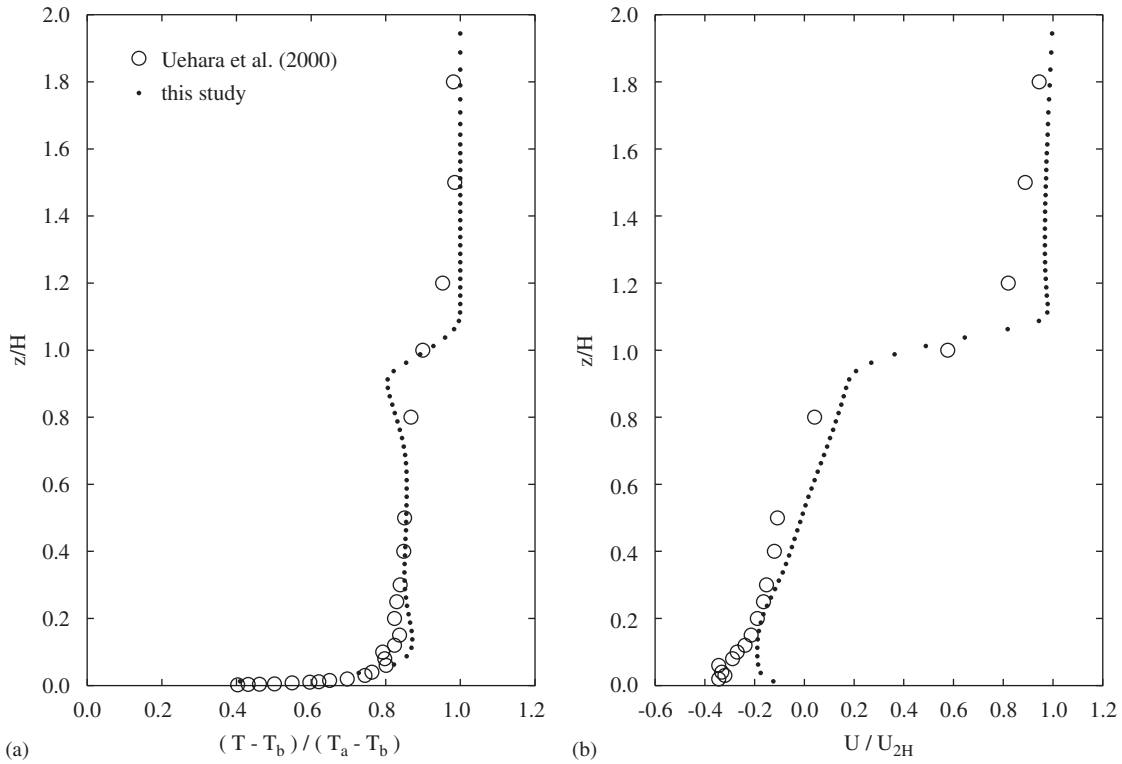


Fig. 10. Vertical profiles of (a) normalized temperature and (b) normalized streamwise horizontal velocity at the center of a street canyon in the present numerical simulation and the wind tunnel experiment of Uehara et al. (2000). $T_b$ is the bottom temperature, $T_a$ the ambient temperature, $H$ the building height, and $U_{2H}$ the streamwise horizontal velocity at the height of $z = 2H$.

Fig. 9 shows that agreement between the numerical simulation and wind tunnel experiment results is overall good. This justifies the accuracy of the present three-dimensional CFD model including the thermodynamic energy equation and the RNG $k-\varepsilon$ turbulence model in simulating street canyon flow (Fig. 10).

## 5. Summary and conclusions

This study examined reactive pollutant dispersion in an urban street canyon with a street aspect ratio of one using a CFD model incorporating simple $NO–NO_2–O_3$ photochemistry. An area emission source of NO and $NO_2$ was considered in the presence of background $O_3$ and street bottom heating ($\Delta T = 5\,^{\circ}C$). It was found that the vortex center meanders over time and in the canyon space and that the time series of the cross-canyon-averaged temperature and reactive pollutant concentrations exhibit a periodicity with temperature being in phase with NO and $NO_2$ concentrations but out of phase with $O_3$ concentration. In the street canyon, the photostationary state defect is small except for near the roof level and the upper downwind region and its local minimum is located near the center of the primary vortex. The budget analysis showed that for NO ($NO_2$) concentration the magnitude of the advection or turbulent diffusion term is much larger (larger) than that of the chemical reaction term, but that for $O_3$ concentration the magnitude of the chemical reaction term is comparable to that of the advection or turbulent diffusion term. The inhomogeneous temperature distribution affects $O_3$ concentration to some extent due to the temperature-dependent photolysis rate and reaction rate constant.

The characteristics of flow and reactive pollutant dispersion in an urban street canyon can vary depending on the degree of street bottom heating. The appearance or disappearance (or absence) of the periodicity in the vortex center location and the averaged temperature and reactive pollutant concentrations with variations in street bottom heating intensity is under investigation. Also, the dependency of the reactive pollutant concentrations on the temperature-dependent photolysis rate and reaction rate constant with variations in street bottom heating intensity is under investigation. Detailed analysis results will be reported in a separate paper. The present CFD model incorporates simple photochemistry, but could be a prototype to develop a CFD model with complex chemical processes for basic and applied research with a wide range of practical applications to urban atmospheric environmental problems. This is a challenging research task.

## Acknowledgments

The authors are very grateful to two anonymous reviewers for providing valuable comments on this work. This research was supported by the Climate Environment System Research Center sponsored by the SRC Program of the Korea Science and Engineering Foundation and also by the Meteorological Research Institute/KMA.

## References

Baik, J.-J., Kim, J.-J., 2002. On the escape of pollutants from urban street canyons. Atmospheric Environment 36, 527–536.

Baik, J.-J., Kim, J.-J., Fernando, H.J.S., 2003. A CFD model for simulating urban flow and dispersion. Journal of Applied Meteorology 42, 1636–1648.

Baker, J., Walker, H.L., Cai, X., 2004. A study of the dispersion and transport of reactive pollutants in and above street canyons—a large eddy simulation. Atmospheric Environment 38, 6883–6892.

Bohnenstengel, S., Schlunzen, K.H., Grawe, D., 2004. Influence of thermal effects on street canyon circulations. Meteorologische Zeitschrift 13, 381–386.

Brown, M.J., Lawson Jr., R.E., DeCroix, D.S., Lee, R.L., 2000. Mean flow and turbulence measurements around a 2-D array of buildings in a wind tunnel. Eleventh Joint Conference on the Applications of Air Pollution Meteorology with the A&WMA, Long Beach, CA, USA, pp. 35–40.

Carpenter, L.J., Clemitshaw, K.C., Burgess, R.A., Penkett, S.A., Cape, J.N., McFadyen, G.G., 1998. Investigation and evaluation of the $NO_x/O_3$ photochemical steady state. Atmospheric Environment 32, 3353–3365.

Castro, I.P., Apsley, D.D., 1997. Flow and dispersion over topography: a comparison between numerical and laboratory data for two-dimensional flows. Atmospheric Environment 31, 839–850.

Caton, F., Britter, R.E., Dalziel, S., 2003. Dispersion mechanisms in a street canyon. Atmospheric Environment 37, 693–702.

DePaul, F.T., Sheih, C.M., 1986. Measurements of wind velocities in a street canyon. Atmospheric Environment 20, 455–459.

Eliasson, I., Offerle, B., Grimmond, C.S.B., Lindqvist, S., 2006. Wind fields and turbulence statistics in an urban street canyon. Atmospheric Environment 40, 1–16.

Hunter, L.J., Johnson, G.T., Watson, I.D., 1992. An investigation of three-dimensional characteristics of flow regimes within the urban canopy. Atmospheric Environment 26B, 425–432.

Jeong, S.J., Andrews, M.J., 2002. Application of the $k-\varepsilon$ turbulence model to the high Reynolds number skimming

flow field of an urban street canyon. Atmospheric Environment 36, 1137–1145.

Kim, J.-J., Baik, J.-J., 1999. A numerical study of thermal effects on flow and pollutant dispersion in urban street canyons. Journal of Applied Meteorology 38, 1249–1261.

Kim, J.-J., Baik, J.-J., 2001. Urban street-canyon flows with bottom heating. Atmospheric Environment 35, 3395–3404.

Kim, J.-J., Baik, J.-J., 2004. A numerical study of the effects of ambient wind direction on flow and dispersion in urban street canyons using the RNG $k-\varepsilon$ turbulence model. Atmospheric Environment 38, 3039–3048.

Liu, C.H., Barth, M.C., 2002. Large-eddy simulation of flow and scalar transport in a modeled street canyon. Journal of Applied Meteorology 41, 660–673.

Liu, H.Z., Liang, B., Zhu, F.R., Zhang, B.Y., Sang, J.G., 2003. A laboratory model for the flow in urban street canyons induced by bottom heating. Advances in Atmospheric Sciences 20, 554–564.

Patankar, S.V., 1980. Numerical Heat Transfer and Fluid Flow. McGraw-Hill, New York, pp. 126–131.

Rotach, M.W., 1995. Profiles of turbulence statistics in and above an urban street canyon. Atmospheric Environment 29, 1473–1486.

Seinfeld, J.H., Pandis, S.N., 1998. Atmospheric Chemistry and Physics. Wiley-Interscience, New York.

Shetter, R.E., Davidson, J.A., Cantrell, C.A., Burzynski Jr., N.J., Calvert, J.G., 1988. Temperature dependence of the atmospheric photolysis rate coefficient for $NO_2$. Journal of Geophysical Research 93, 7113–7118.

Sini, J.-F., Anquetin, S., Mestayer, P.G., 1996. Pollutant dispersion and thermal effects in urban street canyons. Atmospheric Environment 30, 2659–2677.

Tsai, M.Y., Chen, K.S., Wu, C.H., 2005. Three-dimensional modeling of air flow and pollutant dispersion in an urban street canyon with thermal effects. Journal of the Air and Waste Management Association 55, 1178–1189.

Uehara, K., Murakami, S., Oikawa, S., Wakanatsu, S., 2000. Wind tunnel experiments on how thermal stratification affects flow in and above urban street canyons. Atmospheric Environment 34, 1553–1562.

Versteeg, H.K., Malalasekera, W., 1995. An Introduction to Computational Fluid Dynamics: The Finite Volume Method. Longman, Malaysia, pp. 198–203 and 243–244.

Xie, X., Huang, Z., Wang, J., Xie, Z., 2005. Thermal effects on vehicle emission dispersion in an urban street canyon. Transportation Research Part D 10, 197–212.

Yakhot, V., Orszag, S.A., Thangam, S., Gatski, T.B., Speziale, C.G., 1992. Development of turbulence models for shear flows by a double expansion technique. Physics of Fluids A4, 1510–1520.

Zhang, N., Jiang, W.M., Miao, S.G., 2006. A large eddy simulation on the effect of buildings on urban flows. Wind and Structures 9, 23–35.